

Applications of oxygen sensors using smart membranes incorporating polymerized 2,6-dichloroindophenol as a novel method for preventing food spoilage

Tannaz Hasani¹, Hamid Hashemi-Moghaddam^{2*}, Behrouz Akbari-Adergani³

1. Department of Chemical Engineering, Damghan Branch, Islamic Azad University, Damghan, Iran

2. Department of Chemistry, Damghan Branch, Islamic Azad University, Damghan, Iran

3. Ministry of Health and Medical Education, Food and Drug Organization, Iran

* Corresponding author's Email: biotechcellular1983@gmail.com

ABSTRACT

Monitoring molecular oxygen concentrations is critical for many applications, yet developing robust and cost-effective colorimetric sensors capable of detecting color changes remains a longstanding challenge. The current work exhibits the development of an optical oxygen sensor using a smartphone and a sensitive membrane. Radical polymerization was used to coat the surface of silica nanoparticles with a 2,6-dichloroindophenol molecularly imprinted polymer using methacrylic acid, ethylene glycol dimethacrylate, and 2,2'-azobisisobutyronitrile as the functional monomer, cross-linker, and initiator, respectively. After characterizing the imprinted polymers with FTIR, SEM, and XRD, this nanocomposite was impregnated into a PVDF membrane, which changes color when exposed to oxygen. A smartphone's camera was used to identify the color changes using RGB profiling, and this standalone sensor demonstrated good sensitivity. An increasing calibration curve with a linear detection range of 4.79-40 KPa was found by calibrating oxygen samples with slopes for R + G + B pixels. This sensor's suitability for use in food packaging was investigated. The fabricated sensor is very low-cost, easy to use, and can potentially be used in various industries for inexpensive oxygen detection.

Keywords: Oxygen sensor, 2,6-Dichloroindophenol, Imprinted polymer.

Article type: Research Article.

INTRODUCTION

Most food spoilage is primarily caused by oxygen (Castillo-Cambronero *et al.* 2022). Examples of oxidation reactions that degrade food quality include the oxidation of fats, browning reactions, and pigments. Oxygen also spoils many foods due to reactions triggered by enzymes (Mills 2005). Oxidation reduces the nutritional value of some foods while altering their sensory qualities (taste, texture, and aroma). Microorganisms that can contaminate food are active above the freezing point of food, and most common in foods with high water activity (Troller 2012). Additionally, many spoilage organisms grow exponentially faster as the temperature rises, to the point where they can be thermally disrupted or eliminated. Thus, most current, widely used food packaging and storage methods heavily emphasize keeping food chilled in an ambient atmosphere that contains little oxygen (Ashie *et al.* 1996). Packaging for an altered environment is MAP (marketing alternative product) as one of the most popular ideas, which involves adjusting the gas composition inside packages to the ideal levels, effectively maintaining the quality and appearance of the food product, inhibiting microbial growth, and preventing contamination (Bauer *et al.* 2022). Most MAPs are packaged in low oxygen environments (0.5%; Mohan & Ravishankar 2019), except for fresh red meats, for which high O₂ levels (> 40%) contributing to ensure a pleasing appearance and red color (Yang *et al.* 2022; Nethra *et al.* 2023). Control of residual oxygen in vacuum-packaged foods is crucial. Ideally,

it should be applied to every pack, production, and distribution process. Various techniques exist for finding oxygen in vacuum food packaging (Smith *et al.* 1990). Electrochemical, colorimetric redox-based, and phosphorescence-based sensors are the three main methods used to monitor the oxygen concentration in food packaging. The basis of electrochemical sensors is an amperometric, potentiometric, or conductometric reaction. An electrochemical battery without the need for external power sources for oxygen sensing has been developed as an example. It comprises three layers: a zinc sheet (anode), an adhesive gel electrolyte, and an oriented polypropylene film on which silver has been deposited (Won & Won 2021). The use of optical oxygen sensors has gained popularity due to their affordability, ease of miniaturization, ability to be used from a distance, near-noninvasiveness or minimal invasiveness, and, most importantly, the fact that they do not suffer from electrical interference or consume oxygen. The primary principle of colorimetric redox sensors is based on the color change of redox dyes like methylene blue (MB) polyviologen, either with or without oxygen (Roberts *et al.* 2011). However, there are two main issues with these conventional colorimetric redox-based oxygen sensors: (i) they must be created and stored in anaerobic environments due to their propensity to react with ambient air; and (ii) they cease to function after a short time due to the depletion of the reducing agents. To address this issue, more recent research has focused on the design, production, and use of various UV-activated colorimetric redox dyes. So, oxygen colorimetric indicators in the current study, smart membranes imprinted with 2,6-dichloroindophenol (DCIP) were used. Redox coloring: DCIP turns blue when oxidized and brown when it is reduced. The electrochemical redox reaction of DCIP is shown in Fig. 1.

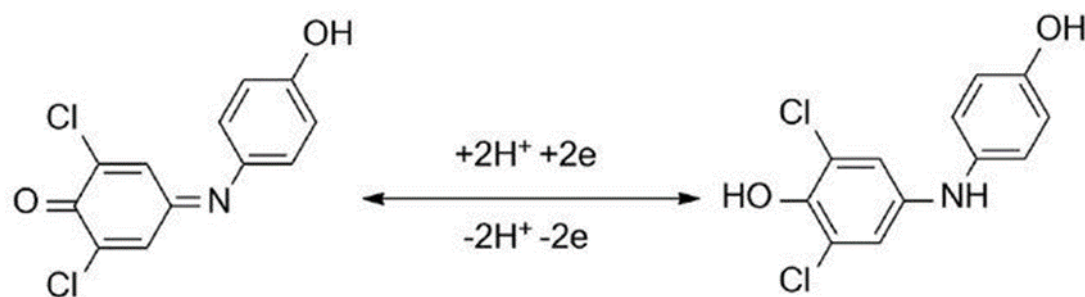


Fig 1. The principle of 2,6-dichlorophenol's redox change.

Molecularly imprinted polymers are widely used in various contexts, including as adsorbents (Hashemi-Moghaddam *et al.* 2013), drug delivery systems (Nazemian *et al.* 2020; Mirzababaei *et al.* 2023) or catalyst (Zhang *et al.* 2019; Muratsugu *et al.* 2020). This ability can accelerate the 2,6-Dichloroindophenol and oxygen kinetic reactions. The effectiveness of a membrane impregnated with 2,6-Dichloroindophenol as a colorimetric oxygen indicator was examined in the current work (Hashemi-Moghaddam *et al.* n.d.).

MATERIALS AND METHODS

Materials

All of the following substances were bought from Merck: 2,2'-azobisisobutyronitrile (AIBN), methacrylic acid (MAA), ethylene glycol dimethacrylate (EGDMA), toluene, MPTS, DMSO, tetra-*n*-butylammonium hydroxide, hydrochloric acid, methanol, ethanol, sodium hydroxide, acetic acid, and acetonitrile. We purchased polyvinylidene fluorid (PVDF) and L 2,6-Dichloroindophenol from Sigma-Aldrich. Analytical-grade chemicals and reagents were all used without further purification. In methanol (12.5%), tetra-*n*-butylammonium hydroxide was diluted. The 99.99% pure nitrogen and oxygen were purchased from Soheil Industrial Gases Co., Tehran, Iran.

Apparatus

The Fourier Transform Infrared (FTIR) spectra of molecularly imprinted and non-imprinted polymers were obtained using a 6700 Thermo Nicolet FTIR spectrometer. IR spectra between 400 and 4000 cm^{-1} were captured. For the morphological study, a Cambridge S-360 scanning electron microscope (SEM) with a 20 kV acceleration voltage assessed the surface of each sample.

Synthesis of modified silica nanoparticles

TEOS was hydrolyzed to prepare the monodispersed spherical silica particles (Peng *et al.* 2010). Following chemical modification with MPTS, the monodispersed silica nanoparticles produced polymerizable double bonds.

Typically, 20 mL of the combined solution was made by mixing 2 mL MPTS and 0.1 g silica nanoparticles with toluene. After 12 hours of refluxing under high-purity nitrogen, the mixture was separated into MPTS-silica nanoparticles, centrifuged, and cleaned with toluene.

Surface coating of silica nanoparticles with 2,6-Dichloroindophenol imprinted polymer

The prearranged solution was made by dissolving MAA (2 mmol), and 2,6-Dichloroindophenol (0.25 mmol) in 25 mL toluene-acetonitrile (4/1, v/v). They were kept in the dark for 12 hours. Through ultrasonic vibration, MPTS-silica nanoparticles (0.1 g) were dissolved in 25 mL toluene-acetonitrile (4/1, v/v). AIBN (1 mmol) and the preset solution (EGDMA, 10 mmol) were then dissolved into the aforementioned solution. While cooling in the ice bath, the mixture was purged for 10 min with high-purity nitrogen. A 300 rpm incubation shaker was used to carry out a three-step temperature polymerization reaction. Pre-polymerization was carried out for six hours at 50 °C before being finished for twenty-four hours at 60 °C. The products were further aged at 75 °C for 6 h after being heated from 60 to 75 °C for 1 hour (at 0.25 °C min⁻¹) to achieve a higher cross-linking density. The resulting polymer was separated from the mixtures using centrifugation. Finally, ethanol solvent was used to clean the obtained nanoparticles by Soxhlet, removing the template. They underwent a methanol rinse and vacuum-assisted room-temperature drying.

Membrane preparation

150 mg fructose was dissolved in 2 mL water, then 3.5 mL 2,6-dichloroindophenol solution (40 mg in 100 mL of 96% ethanol) was added. 150 mg PVDF, 10 mg 2,6-dichloroindophenol imprinted polymer, and 2 mL DMSO were added to the above mixture. After sonication for 10 min, the mixture was transferred to a 100-mL beaker, and the beaker contents were dried for 5 hours on a heater stirrer at 70 °C (Benabid *et al.* 2020).

Membrane reduction reaction

150 mg fructose was dissolved in 2 mL water with 3 mL 2,6-dichlorophenolindophenol solution, and 0.1 mL tetra-n-butylammonium hydroxide was transferred to a 5-mL syringe. The membrane prepared in the previous step was quickly transferred to the syringe, and the air was removed completely. After 12 hours, the membrane was ready to use.

Control of oxygen concentration

The oxygen indicator membrane was attached to the inner side of the polyethylene pouches, which could then be filled with nitrogen or various oxygen gas pressures.

Development of a smartphone RGB profiling app

Using our own Android app for smartphones (Color Detector & Catcher TM), we could determine the sensor's RGB profile concerning oxygen concentration. The application determined RGB pixels, and these data were then used to create the calibration curve. An indicator was added to the adsorbent to estimate the oxygen levels using the app, and the adsorbent was then placed close to the smartphone camera (Soni & Jha 2017).

Oxygen sensor measurements, detailed characterization of sensors

Full oxygen calibrations (0-100 kPa) were performed at 10, 20, and 30 °C as part of the detailed characterization. These circumstances cover the primary oxygen and storage temperature ranges for packaged goods and, consequently, for sensor operation. To determine the actual oxygen pressure, RGB values obtained for each of the oxygen pressures were recorded. Our mobile RGB profiling app examined the color change on the adsorbent. Excel software was used to plot calibration curves after measuring different oxygen pressures in terms of changes in slope for the red (R), green (G), and blue (B) pixel colors. Combinations of these colors were also used (total pixel changes for R + G + B), and calibration curves were obtained against the oxygen concentration of each of these combinations separately to increase sensitivity. R, G, and B together form an additive model of color change. Data was plotted to represent the standard deviation after five calibration runs.

RESULTS AND DISCUSSION

Characterization of sensor materials

FT-IR was used to characterize the synthesized polymers with molecular imprints. Si-O-Si stretching vibrations were linked to a peak at 653.47 cm⁻¹ in the FTIR spectra of synthetic polymer, and a weak band is responsible for the bending mode (at 481.1 cm⁻¹; Tran *et al.* 2013). The absorptions in the IR spectra were observed owing to

carbonyl group stretch (ca. 1702 cm^{-1}), carboxyl OH stretch (ca. 3442 cm^{-1}), C—O stretch (ca. 1068 cm^{-1}), and C—H vibrations (ca. 898 , ca. 1405 , ca. 1472 , and ca. 2972 cm^{-1}). The FT-IR spectra of synthesized molecularly imprinted polymer are shown in Fig. 2.

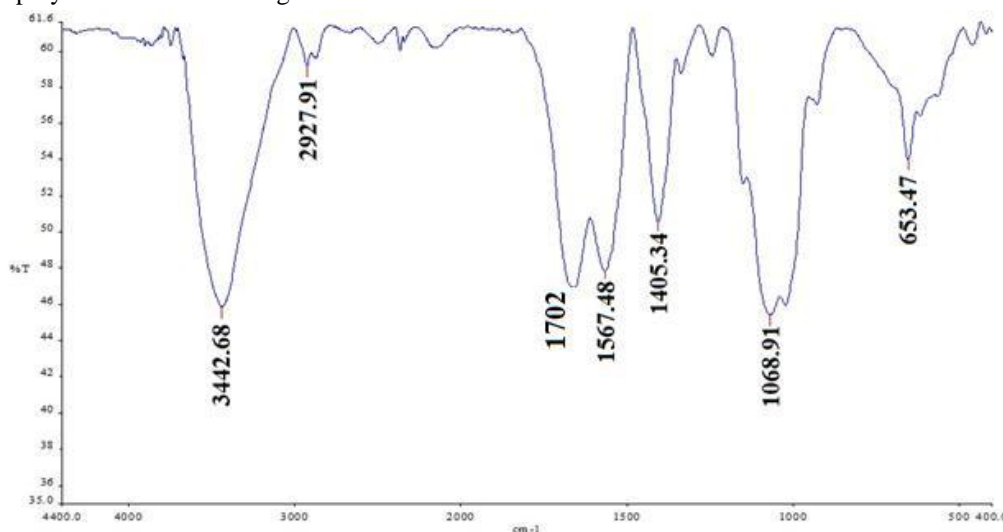


Fig. 2. The FTIR spectra of MIP of synthesized L-2,6-Dichloroindophenol imprinted polymer.

The XRD spectrum and SEM image of the synthetic 2,6-Dichloroindophenol imprinted polymer are shown in Figs. 3 and 4, respectively. The synthetic molecularly imprinted polymer is monodispersed and uniform, as the SEM image shows. Furthermore, silica is indicated by the observed XRD peak in $2\theta=26^\circ$ spectra. Also, the uniform synthesis of molecularly imprinted polymer and unbroken holes in the membrane is apparent in SEM images. In EDAX image of the synthesized membrane, silica, C, O, and F can be detected (Fig. 5).

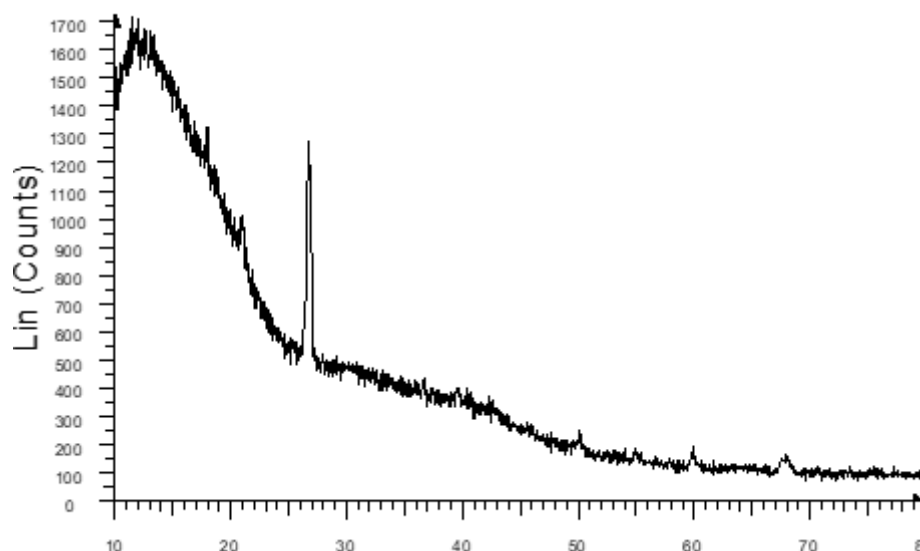


Fig. 3. The synthetic 2,6-Dichloroindophenol imprinted polymer's XRD pattern.

Interference in the oxygen sensor response

Numerous factors, such as ambient light and the position of a smartphone camera, can affect how an oxygen sensor responds. Studies have been conducted to determine the effect of each of these parameters on sensor response. Many different research methods have examined how ambient light affects sensor response. Even though the slope method reduces interference from outside light to some extent, the best conditions must be chosen to obtain accurate results, because ambient light is a significant source of error in smartphone-based optical sensing. According to the findings of our preliminary studies, the attached mode (membrane attached to a smartphone camera) produced the maximum sensor response. In contrast, ambient light (flashlight on) and inside a dark box (flashlight on) produced slightly different pixel intensities. The membrane was out of focus concerning

the camera because it was physically stuck, which was the attached mode's main flaw. The flashlight can illuminate the paper more intensely than ambient light because it can diffuse through the wet white membrane. This might explain why the sensor response varies less in this mode.

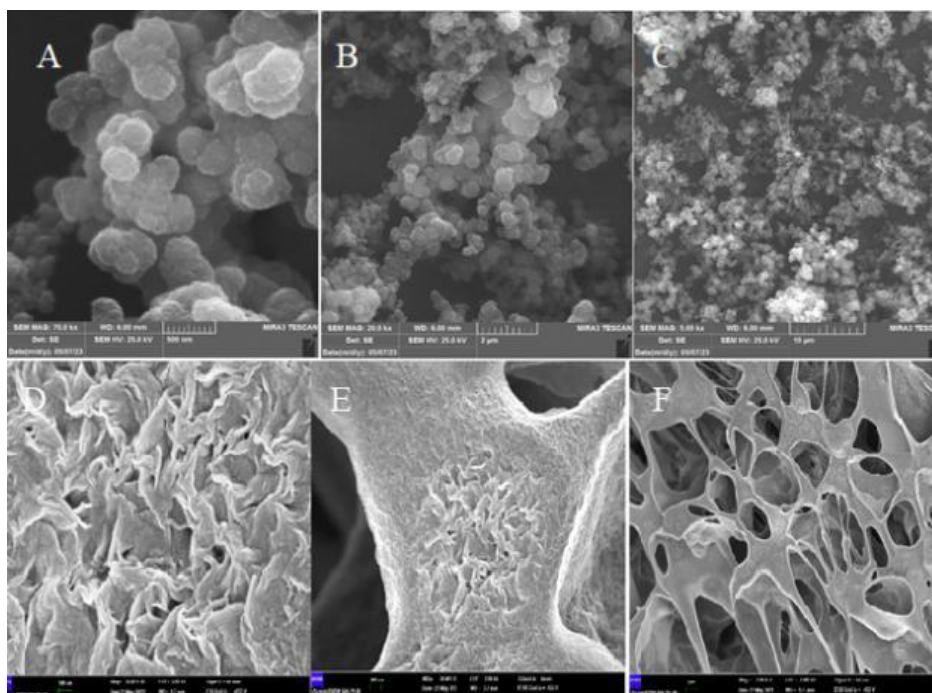


Fig. 4. SEM images of The 2,6-Dichloroindophenol imprinted polymer (A, B, C, at 135kx, 2kx and 5 kx, respectively) and imprinted polymer impregnated in PVDF (D, E and F, 50, 30 kx and 5 kx).

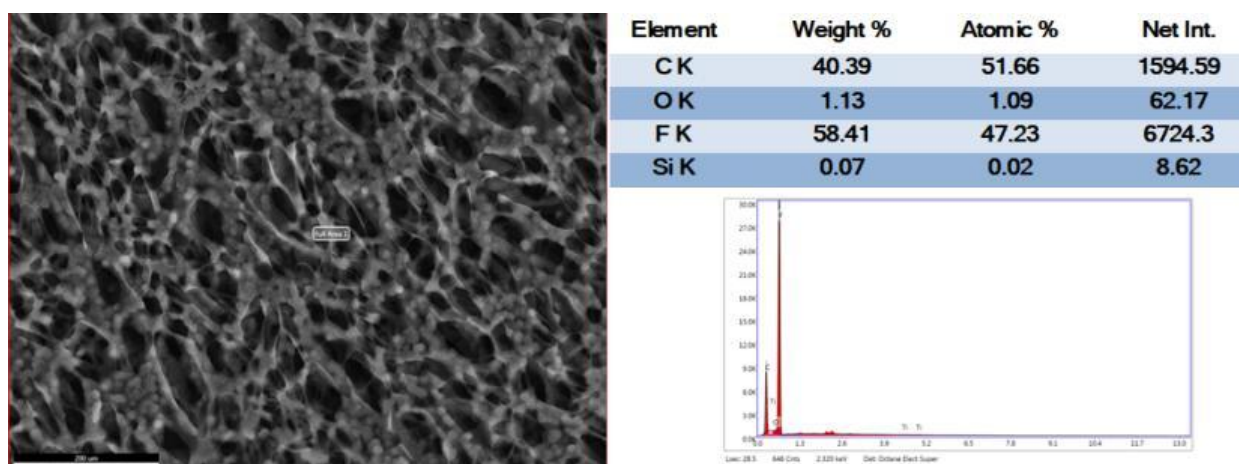


Fig. 5. The 2,6-Dichloroindophenol imprinted polymer images from the EDAX analysis of the synthetic PVDF.

Additionally, there was a chance of error in ambient light, mainly if there was a sharp change in light intensity, as would occur if the user suddenly moved from a well-lit room area to a darker corner during the measurement. It was also tested to see how different smartphone models affected sensor responses. Most smartphone brands have different camera modules made by different manufacturers with different specifications, which can cause variations in sensor measurements. Three different smartphone models, the Xiaomi Poco C40, the Samsung Galaxy S4, and the Samsung Galaxy A13 were used for the experiment. The attached mode was used to conduct the study. Compared to smartphone models, there was only a slight change in pixel intensity. In addition to the smartphones mentioned above, any smartphone with a 5-megapixel camera or higher can be used for oxygen estimation. Finally, the oxygen sensor was subjected to tests to determine its reproducibility. When readings were obtained for five different samples over three days, it was discovered that the sensor had an 87% reproducibility. Comparing the developed strip's price to other commercially available oxygen sensors, it was also cheaper (about

\$1), and during mass production, it could be even less expensive. Any smartphone model with at least a 5-megapixel camera and an integrated flashlight can be used for oxygen sensing.

Oxygen sensor measurements

2,6-dichloroindophenol-imprinted polymer impregnated on the PVDF membrane was used in the tests. The formation of an oxidized form in the presence of oxygen caused the membrane to change color. The oxidation rate increased by elevating oxygen pressure, resulting in a more pronounced color change (Fig. 6). Calibration curves were obtained for the change in slope for R, G, and B pixels concerning oxygen pressure. Exponentially increasing curves about oxygen were found for all of R, G, and B (Figs. 7, 8, and 9). The calibration curves for R + G + B concerning oxygen concentration were also plotted to improve sensitivity (Fig. 10). Other studies on the oxygen sensor were conducted by plotting slope R + G + B against oxygen concentration. Of these combinations, R + G + B provided the maximum response. The response time was set at 4 minutes.

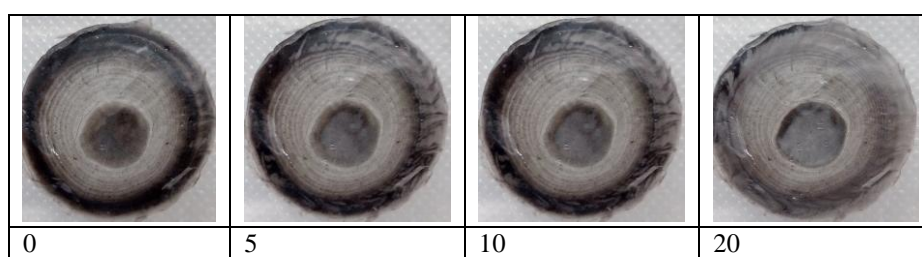


Fig 6. Color change of smart membrane against oxygen pressure

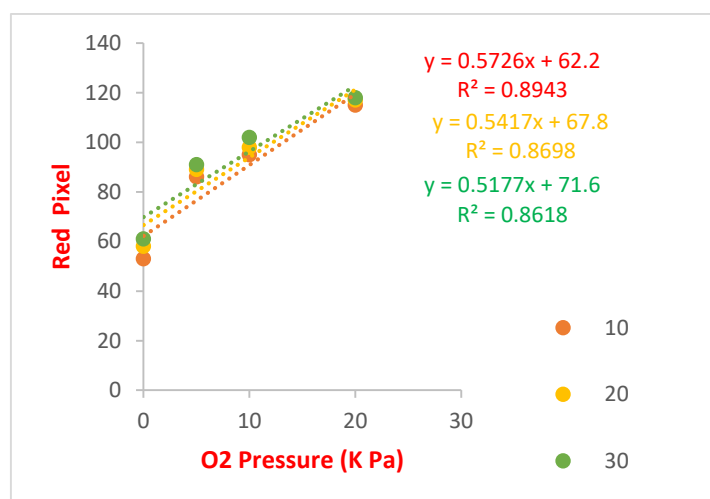


Fig. 7. Calibration curve for change in slope for red pixels for oxygen pressure.

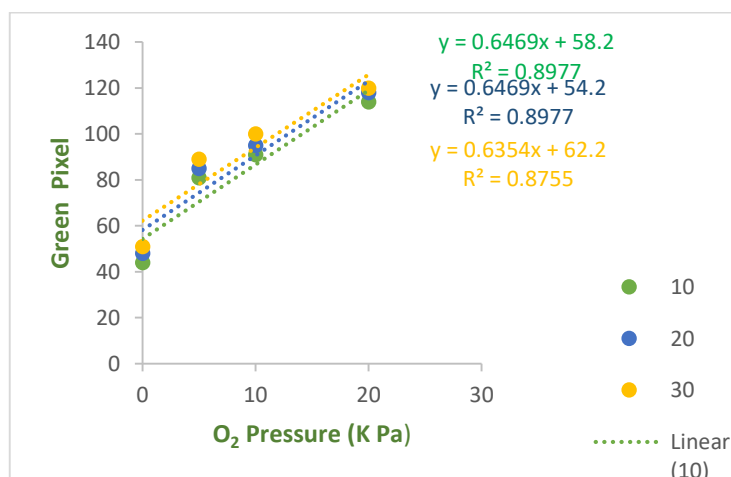


Fig 8. Calibration curve for change in slope for green pixels with respect to oxygen pressure.

The concentration at which the sensor's signal-to-noise ratio is just above 3 is typically used to determine the oxygen sensor's limit of detection (Soni & Jha 2017). The calibration curve was linear in the range of 4.79-40 KPa. However, it can also be determined practically by observing the variation in slope $R + G + B$ for samples devoid of oxygen. For this purpose, the nitrogen package is permitted to make contact with the oxygen sensor. It was discovered that the sensor noise level for this sample was 9 pixels/sec ($n = 6$), which is equivalent to 1,29 KPa at 20 °C. Finally, the applicability of sensor was examined in different vacuum food packaging samples and color change could be seen in damaged samples.

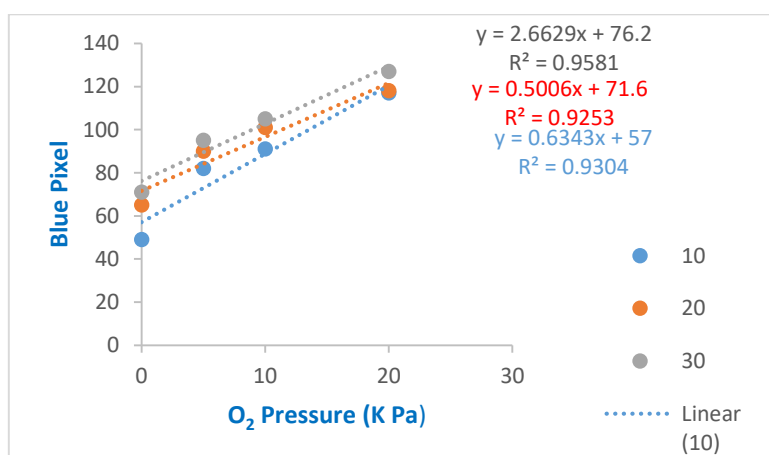


Fig. 9. Calibration curve for change in slope for blue pixels with respect to oxygen pressure.

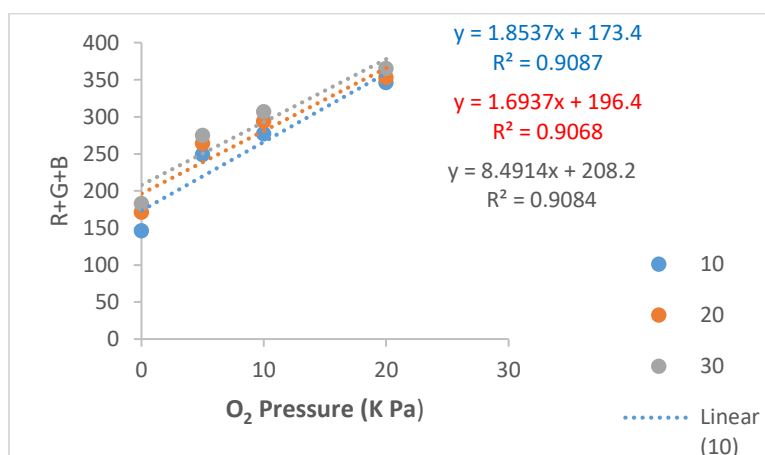


Fig. 10. Calibration curve for change in slope for red + green + blue pixels with respect to oxygen pressure.

CONCLUSION

In the current study, an optical oxygen sensor for smartphones has been developed to estimate oxygen levels. The sensor was made using a straightforward methodology by immobilizing 2,6-dichloroindophenol imprinted polymer, fructose, and 2,6-Dichloroindophenol in PVDF membrane. Using RGB profiling and our custom smartphone application built using the slope method, we determined the color change to oxygen concentration. Since the polymeric sensor is so sensitive and reasonably priced, the system has much potential for detecting oxygen with the naked eye in real-time.

ACKNOWLEDGMENTS

We appreciate the Laboratory Complex of Islamic Azad University, Damghan Branch, Damghan, Iran, helpful technical support. And this paper is self-funded.

REFERENCES

- Ashie, INA, Smith, JP, Simpson, BK & Haard, NF 1996, Spoilage and shelf-life extension of fresh fish and shellfish. *Critical Reviews in Food Science & Nutrition* 36: 87-121.
- Bauer, AS et al. 2022, Cereal and confectionary packaging: Background, Application and shelf-life extension.

- Foods*, 11: 697.
- Benabid, FZ, Kharchi, N, Zouai, F & Benachour, D 2020, Effect of solvent type, conditions of dissolution and evaporation temperature on crystallinity phases of PVDF. *Journal of Polymer Science and Technology*, (ISSN: 2550-1917), 5: 47–51.
- Castillo-Cambronero, G *et al.* 2022, Use of nanosensor technologies in the food industry. *Nanosensors for Smart Agriculture*: 643-655.
- Hashemi-Moghaddam, Hamid, Tannaz Hasani, and Behrouz Akbari-Adergani. "Preparation of Smart Membrane Incorporated by 2, 6-Dichloroindophenol Imprinted Polymer as an Oxygen Sensor in Food Packaging." *Available at SSRN 4637578*.
- Hashemi-Moghaddam, H, Rahimian, M & Niromand, B 2013, Molecularly imprinted polymers for solid-phase extraction of sarcosine as prostate cancer biomarker from human urine. *Bulletin of the Korean Chemical Society*, 34(8): 2330–2334.
- Mills, A 2005, Oxygen Indicators and Intelligent Inks for Packaging Food. *Chemical Society Reviews*, 34(12): 1003–1011.
- Mirzababaei, M *et al.* 2023, Graphene quantum dots coated cationic polymer for targeted drug delivery and imaging of breast cancer. *Journal of Polymer Research* 30(7): 268.
- Mohan, CO & Ravishankar, CN 2019, Active and Intelligent packaging systems-Application in seafood.
- Muratsugu, S, Sora SH & Mizuki, T, 2020, Recent progress in molecularly imprinted approach for catalysis. *Tetrahedron Letters*, 61(11): 151603.
- Nazemian, M *et al.* 2020, Immobilized peptide on the surface of Poly L-DOPA/Silica for Targeted delivery of 5-fluorouracil to breast tumor. *International Journal of Peptide Research and Therapeutics* 26: 259-269.
- Nethra, PV *et al.* 2023, Critical factors affecting the shelf life of packaged fresh red meat—A review. *Measurement: Food*, 10: 100086.
- Peng, Y *et al.* 2010, Molecularly Imprinted polymer layer-coated silica nanoparticles toward dispersive solid-phase extraction of trace Sulfonylurea herbicides from soil and crop samples. *Analytica chimica acta* 674(2): 190–200.
- Roberts, L, Lines, R, Reddy, S & Hay, J 2011, Investigation of polyviologens as oxygen indicators in food packaging. *Sensors and Actuators B: Chemical* 152: 63-67.
- Smith, JP, Hosahalli SR & Benjamin K S 1990, Developments in food packaging technology. Part II, Storage aspects. *Trends in Food Science & Technology* 1: 111–118.
- Soni, A & Sandeep, KJha 2017, Smartphone based non-invasive salivary glucose biosensor. *Analytica Chimica Acta* 996: 54-63.
- Tran, TN, Thi, VAP, My, LPL & Thi Phuong, TN 2013, Synthesis of amorphous silica and sulfonic acid functionalized silica used as reinforced phase for polymer electrolyte membrane. *Advances in Natural Sciences: Nanoscience and Nanotechnology* 4(4): 45007.
- Troller, J 2012, Water Activity and Food. Elsevier.
- Won, S, & Won, K 2021, Self-powered flexible oxygen sensors for intelligent food packaging. *Food Packaging and Shelf Life*, 29: 100713.
- Yang, J *et al.* 2022, Investigation of the relationship between microbiota dynamics and volatile changes in chilled beef steaks held under high-oxygen packaging enriched in carbon dioxide. *Meat Science*, 191: 108861.
- Zhang, Z, Yuqing, L, Zhang, X & Liu, J 2019, Molecularly imprinted nanozymes with faster catalytic activity and better specificity. *Nanoscale* 11(11): 4854-4863.

Bibliographic information of this paper for citing:

Hasani, T, Hashemi-Moghaddam, H, Akbari-Adergani, B 2024, Applications of oxygen sensors using smart membranes incorporating polymerized 2,6-dichloroindophenol as a novel method for preventing food spoilage. *Caspian Journal of Environmental Sciences*, 22: 147-154.